Eur. Phys. J. A (2019) **55**: 92
DOI 10.1140/epja/i2019-12753-y

THE EUROPEAN PHYSICAL JOURNAL A

Review

Verification of R-matrix calculations for charged-particle reactions in the resolved resonance region for the ^{7}Be system

Ian J. Thompson[1], R.J. deBoer[2,3], P. Dimitriou[4,a], S. Kunieda[5], M.T. Pigni[6], G. Arbanas[6], H. Leeb[7], Th. Srdinko[7], G. Hale[8], P. Tamagno[9], and P. Archier[9]

[1] Lawrence Livermore National Laboratory, L-414, Livermore, CA 94551, USA
[2] The Joint Institution of Nuclear Astrophysics, University Notre Dame, Notre Dame, IN 46556, USA
[3] Department of Physics, University Notre Dame, Notre Dame, IN 46556, USA
[4] Division of Physical and Chemical Sciences, International Atomic Energy Agency, Wagramerstrasse 5, Vienna A-1400, Austria
[5] Japan Atomic Energy Agency, Tokai 319-1195, Japan
[6] Oak Ridge National Laboratory, PO Box 2008, Oak Ridge, TN 37831, USA
[7] Atominstitut, Technische Universität Wien, Wiedner Hauptstrasse 8-10, A-1040 Vienna, Austria
[8] Los Alamos National Laboratory, Theoretical Division, Los Alamos, NM 87545, USA
[9] CEA-DEN Cadarache, DER/SPRC/LEPh, F-13108 Saint-Paul-lez-Durance, France

Received: 15 February 2019 / Revised: 4 April 2019
Published online: 17 June 2019

Communicated by N. Alamanos

Abstract. R-matrix theory is used to describe nuclear reactions in the resolved resonance region. It uses information on bound states and low energy resonances to accurately parametrize cross sections on the resonances as well as the non-resonant background. Since the seminal work of Lane and Thomas (1958), the approach has been widely used to analyze experimental cross-section data in a broad range of fields spanning nuclear reaction dynamics, nuclear astrophysics, ion beam analysis and their applications. Different R-matrix codes have been developed and used in these different applications with very little communication among the developers or practitioners on the capabilities, achievements or limitations of the codes. A limited comparison among three R-matrix codes on neutron-induced reactions was performed by the International Atomic Energy Agency (IAEA) International Evaluation of Neutron Cross Section Standards project (2007). Since then, significant progress has been made in their implementation of the R-matrix algorithms, and R-matrix codes have enhanced capabilities. In this paper we present, for the first time, the results of a comprehensive effort to verify the most widely used R-matrix codes in the various fields of nuclear science and applications: AMUR, AZURE2, CONRAD, EDA, FRESCO, GECCCOS, and SAMMY. In addition to the description of the capabilities of the codes and their specifications, we discuss the results of a joint exercise which was coordinated by the International Atomic Energy Agency. The aim of the exercise was to compare calculations of charged-particle reaction cross sections for the light composite system ^{7}Be. The calculations were performed by the codes using identical input R-matrix parameters and other specifications and were limited to charged-particle channels.

1 Introduction

Charged-particle induced reactions at low energies are important for Ion Beam Analysis (IBA) applications such as materials analysis, cultural heritage and preservation, environmental and climate control, and forensics, to mention a few examples. For over 10 years, the International Atomic Energy Agency has been serving as the international center for the collection and dissemination of nuclear data for IBA. Through a series of Coordinated Research Projects (CRP) [1,2], collaborations with expert scientists and staff efforts, it has created and maintained the Ion Beam Analysis Data Library (IBANDL) [3,4] that contains over 3000 datasets of differential and total experimental cross sections for charged-particle induced reactions in the low energy region below several MeV. Evaluated cross-section data are also crucial for the implementation of the ion beam analytic techniques, since they are used in computer simulations of thick targets which are then compared to measured spectra of the emitted radiation (particle or gamma). For many years the IBA community has relied on one single source of evaluated differential cross sections: the SigmaCalc online calculator.

[a] e-mail: P.Dimitriou@iaea.org

The cross sections available on this website are R-matrix fits/evaluations performed by Gurbich [5].

On the other hand, the evaluated data files (ENDF/B, JEFF, JENDL, ROSFOND etc) collected by nationally or internationally coordinated efforts are, to date, incomplete as far as charged-particle induced reactions in the resolved resonance region are concerned. In several cases, the data files contain cross sections that have been extrapolated from data evaluated at higher energies where cross sections are smooth and are described by a statistical model.

However, with the emergence of new applications and developments in existing applications, the need for reliable charged-particle induced reactions at low energies is growing. One example is the management of fuel in nuclear reactors involving the control of neutrons produced after the reactor operation is shut down. For the most widely used fuel materials, UO_2, UF_6, PuF_4 and PuO_2, the dominant neutron producing reactions are $(\alpha, x\mathrm{n})$ reactions on isotopes of O and F. The alpha-particles are produced from the decay of heavy isotopes and are stopped or reabsorbed in the reactor fuel through interactions with the lighter elements. At energies above the neutron emission threshold, $(\alpha, x\mathrm{n})$ reactions may occur in the resolved resonance region. A survey of the evaluated libraries reveals a lack of reliable $(\alpha, x\mathrm{n})$ data in the low-energy resolved resonance region [6].

Another area of science where low-energy charged-particle reactions are important is nuclear astrophysics. The main stellar processes that are responsible for energy production in stars and lead to the synthesis of the light and medium-mass elements up to the iron nuclei, are fueled by thermonuclear reactions at temperatures of tens of millions of Kelvin. In laboratories here on earth these conditions translate into charged-particle induced reactions on light and medium-mass nuclei at energies of a few tens of keV. Significant effort has been made over the past decades to measure these cross sections at higher energies where the reaction yields are large enough to observe, and provide theoretical descriptions, R-matrix fits and/or evaluations of the data. The latter are important for extrapolating to the lower energies needed for the stellar nucleosynthesis models. Several astrophysics dedicated-compilations (NACRE-I [7] and II [8]) and databases (REACLIB [9], BRUSLIB [10], KADONIS [11], NUCASTRODATA.ORG [12]) have been made available as a result. The knowledge that has been accumulated over the years in measuring, fitting and modelling charged-particle induced reactions for astrophysics applications could be extremely useful for other applications and should, therefore, be integrated in the current effort to make complete and reliable evaluated nuclear data files for charged-particle induced reactions available to the broader user community.

Apart from the gaps in the charged-particle evaluated data in the resolved resonance region, there are other outstanding issues regarding reaction mechanisms in the low-energy region that affect both neutron- and charged particle-induced reactions. These include such questions as how to extend R-matrix theory to higher energies where a large number of channels are open, how to transition smoothly and consistently from the resolved resonance region to the statistical model region, and how to go beyond the particle dissociation thresholds. These issues are still not well understood and so require broader international collaboration among experts.

In response to the emerging data needs, the IAEA is coordinating an international effort to address all the outstanding issues related to the evaluation of charged-particle reactions in the resolved resonance region [13–16]. The coordinated project's goal is to compare the available R-matrix codes and create a common platform where input and output resonance parameters can be exchanged by the different R-matrix codes, independent of the specific formats and approximations used. An intercomparison of three R-matrix codes, namely EDA, RAC and SAMMY, was previously performed under the IAEA International Evaluation of Neutron Cross Section Standards project [17], however it was of a more limited scope. The present comparison focuses first on the R-matrix algorithms, how they are implemented and what approximations are made. In particular, specific issues such as the impact of relativistic or non-relativistic kinematics, unitarity and boundary conditions are explored in depth. To this end, an exercise was assigned to the participants of the project, to calculate the R-matrix cross sections for a given system, ^{7}Be, using the same set of well-defined conditions. The calculations were limited to charged-particle channels only.

In this paper, we present the systematic comparison of the R-matrix codes AMUR, AZURE2, EDA, FRESCOX, SAMMY, GECCCOS and CONRAD, and discuss some of the approximations implemented in them as well as the results of the joint exercise. In sect. 2 we present the main principles of R-matrix theory and how it is implemented. Kinematics, unitarity and boundary conditions and alternative representations are discussed. In sect. 3 we compare the R-matrix codes and their capabilities. In sect. 5, we present the results of a joint exercise whose goal was to verify that the R-matrix codes produce the same cross sections when using identical input parameters and conditions for a light system, ^{7}Be, involving only charged-particle channels. Our conclusions are given in sect. 6.

2 R-matrix theory, approximations and representations

2.1 General R-matrix theory

R-matrix theory was introduced [18] as a method to solve, for each spin-parity group J^π, the set of N coupled Schrödinger equations

$$[T_\alpha(R_\alpha) + U_\alpha - E_\alpha]\,\psi_\alpha(R_\alpha) + \sum_{\beta\neq\alpha}^{N} V_{\alpha\beta}\psi_\beta(R_\beta) = 0, \quad (1)$$

for a set of two-body channels α with a specified Hamiltonian $H = T + U + V$, where the component V couples different channels. The kinetic energy operator is

$T_\alpha(R_\alpha) = -t_\alpha \frac{\mathrm{d}^2}{\mathrm{d}R_\alpha^2}$ where $t_\alpha = \hbar^2/2\mu_\alpha$ with μ_α the reduced mass. We assume that the diagonal U and off-diagonal V potentials are zero outside some radial distance a_α in each channel, except for the $1/R$ Coulomb component.

We look for solutions which satisfy, at some external radius $R_\alpha \geq a_\alpha$, the boundary conditions given in terms of Coulomb wave functions $H_\ell^\pm(\rho) = G_\ell(\rho) \pm iF_\ell(\rho)$,

$$\psi^{J\pi}_{\alpha\alpha_\mathrm{i}}(R_\alpha) = \frac{i}{2}\left[H_\ell^-(k_\alpha R_\alpha)\,\delta_{\alpha\alpha_\mathrm{i}} - H_\ell^+(k_\alpha R_\alpha)\,\mathsf{S}^{J\pi}_{\alpha\alpha_\mathrm{i}}\right], \quad (2)$$

where k_α are the wave numbers, $\rho = k_\alpha a_\alpha$, α_i is the incoming channel, and $\mathsf{S}^{J\pi}_{\alpha\alpha_\mathrm{i}}$ is the S matrix used to make the cross sections.

In the "computational R-matrix method" [19], the Hamiltonian is diagonalized inside the radial ranges $[0, a_\alpha]$. In order to obtain orthonormal eigenwavefunctions, the Hamiltonian is supplemented by the Bloch operators

$$\hat{B}_\alpha = \delta(R_\alpha - a_\alpha)\left(\frac{\mathrm{d}}{\mathrm{d}R_\alpha} - \frac{B_\alpha}{R_\alpha}\right)$$

for some constants B_α which may be different in each channel, but independent of energy. Let $\Phi^p_\alpha(R_\alpha)$ be the eigenfunctions at eigenenergies e_p. Of these eigenenergies, negative energies are associated with the bound state energies of the composite nuclear system, and positive energies associated with both narrow and broad resonances in the continuum. The pole energies e_p are therefore bounded below by the system binding energy, and extend to indefinitely large positive values in general.

The S matrix may then be determined from the asymptotic amplitudes of these eigen-solutions, by means of an intermediate R matrix. We define *reduced width amplitudes* for each channel α and pole p in proportion to the tail amplitudes of these eigen-solutions, as

$$\gamma_{p\alpha} = \sqrt{\frac{t_\alpha}{a_\alpha}}\,\Phi^p_\alpha(a_\alpha) = \sqrt{\frac{\hbar^2}{2\mu_\alpha a_\alpha}}\,\Phi^p_\alpha(a_\alpha). \quad (3)$$

From these, the R matrix R is the sum over the infinite set of pole energies, with elements

$$\mathsf{R}_{\alpha\alpha'}(E) = \sum_{p=1}^{\infty} \frac{\gamma_{p\alpha}\gamma_{p\alpha'}}{e_p - E}\,, \quad (4)$$

from which the scattering S matrix follows as

$$\mathsf{S} = \frac{\mathbf{t}^{\frac{1}{2}}\mathbf{H}^+ - \mathbf{R}\,\mathbf{t}^{\frac{1}{2}}(\mathbf{a}\mathbf{H}^{+\prime} - \mathbf{B}\mathbf{H}^+)}{\mathbf{t}^{\frac{1}{2}}\mathbf{H}^- - \mathbf{R}\,\mathbf{t}^{\frac{1}{2}}(\mathbf{a}\mathbf{H}^{-\prime} - \mathbf{B}\mathbf{H}^-)}\,. \quad (5)$$

where $\mathbf{a}$, $\mathbf{t}$ and $\mathbf{B}$ are the diagonal matrices of a_α, t_α and B_α values respectively. The derivatives $\mathbf{H}^{\pm\prime}$ are with respect to radii $\boldsymbol{R}_\alpha$.

2.2 Phenomenological R-matrix theory

The "phenomenological R-matrix method" [19] that is followed in the remainder of this paper does not start from a Hamiltonian and does not have an infinite series of poles. Rather it uses a finite number P of R-matrix pole energies e_p, with reduced width amplitudes $\gamma_{p\alpha}$, as parameters in the familiar finite sum

$$\mathsf{R}_{\alpha\alpha'}(E) = \sum_{p=1}^{P} \frac{\gamma_{p\alpha}\gamma_{p\alpha'}}{e_p - E}\,, \quad (6)$$

to be adjusted to fit experimental scattering data. Positive-energy poles are again aligned with scattering resonances. Other poles are "background poles" at higher positive energies to attempt to represent the effects of all the remaining terms missing in comparison with eq. (4).

2.3 Simplified formulation

Equation (5) is often easier to calculate if we simplify it as follows. We define a "logarithmic derivative" matrix

$$\mathbf{L} = \mathbf{H}^{+\prime}/\mathbf{H}^+ - \mathbf{B}/\mathbf{a} = (\boldsymbol{S} + i\mathbf{P} - \mathbf{B})/\mathbf{a}, \quad (7)$$

where the penetrability $\mathbf{P}$ and shift function $\boldsymbol{S}$ are taken as matrices with diagonal elements

$$P_\alpha = k_\alpha a_\alpha/(F_\alpha^2 + G_\alpha^2) \quad (8)$$

$$\text{and} \quad S_\alpha = (\dot{F}_\alpha F_\alpha + \dot{G}_\alpha G_\alpha)P_\alpha. \quad (9)$$

The derivatives $\dot{F}$ are with respect to ρ. Since $\mathbf{H}^{-\prime}/\mathbf{H}^- = \mathbf{L}^*$ and $P_\alpha = k_\alpha a_\alpha/(H_\alpha^+ H_\alpha^-)$, we have

$$\mathbf{S} = \boldsymbol{\Omega}\frac{1}{\sqrt{\mathbf{t}\mathbf{H}^-\mathbf{H}^+}}[1 - \mathbf{a}\mathbf{R}\mathbf{L}]^{-1}[1 - \mathbf{a}\mathbf{R}\mathbf{L}^*]\sqrt{\mathbf{t}\mathbf{H}^-\mathbf{H}^+}\,\boldsymbol{\Omega} \quad (10)$$

where $\boldsymbol{\Omega}$ is the matrix with diagonal elements $e^{i\phi_\alpha}$ for hard-sphere phase shifts

$$\tan\phi_\alpha = -F_\alpha/G_\alpha. \quad (11)$$

The matrix product $\mathbf{t}\mathbf{H}^-\mathbf{H}^+$ is diagonal, with

$$(\mathbf{H}^-\mathbf{H}^+\mathbf{t})_\alpha = (F_\alpha^2 + G_\alpha^2)\frac{\hbar^2}{2\mu_\alpha} = \frac{k_\alpha a_\alpha}{P_\alpha}\frac{\hbar^2}{2\mu_\alpha} = \frac{\hbar v_\alpha a_\alpha}{2P_\alpha}\,, \quad (12)$$

using the diagonal matrix of channel velocities $\mathbf{v} = \{\hbar k_\alpha/\mu_\alpha\}$. The symmetric matrix $\tilde{\mathbf{S}}$ with velocity factors is $\mathbf{v}^{\frac{1}{2}}\mathbf{S}\mathbf{v}^{-\frac{1}{2}}$, giving

$$\begin{aligned}\tilde{\mathbf{S}} &= \boldsymbol{\Omega}\mathbf{P}^{\frac{1}{2}}[1 - \mathbf{a}\mathbf{R}\,\mathbf{L}]^{-1}[1 - \mathbf{a}\mathbf{R}\,\mathbf{L}^*]\mathbf{P}^{-\frac{1}{2}}\boldsymbol{\Omega},\\ &= \boldsymbol{\Omega}[1 + 2i\mathbf{P}^{\frac{1}{2}}(1 - \mathbf{a}\mathbf{R}\mathbf{L})^{-1}\mathbf{R}\mathbf{P}^{\frac{1}{2}}]\boldsymbol{\Omega}, \quad (13)\end{aligned}$$

the last form being widely used.

2.4 Non-relativistic and relativistic kinematics

Consider a channel α with a projectile of mass m_p and charge Z_p incident at laboratory energy E_p on a target of mass m_t and charge Z_t. We need in R-matrix theory to calculate the relative velocities $v_\alpha = \beta_\alpha c$, reduced masses μ_α, wave numbers k_α, and Sommerfeld parameters $\eta_\alpha = Z_p Z_t e^2/\hbar v_\alpha \equiv Z_p Z_t \alpha_f/\beta_\alpha$ in order to calculate the Coulomb functions and the kinematic factors in the cross sections. The total mass is $M = m_p + m_t$. The α_f is the fine structure constant, given with other constants in table 2.

Most of our codes use non-relativistic kinematics, where we calculate:

center-of-mass energy	$E_{cm} = \frac{m_t}{M} E_p$,
reduced mass	$\mu_\alpha = m_p m_t / M$,
fraction of light speed	$\beta_\alpha = \sqrt{2E_{cm}/\mu_\alpha c^2}$,
wave number	$k_\alpha = \beta_\alpha \, \mu_\alpha c^2/\hbar c$.

The EDA code has an option for relativistic kinematics, which starts with the invariant square of the total 4-momentum $s = M^2c^2 + 2m_t E_p$. The energy in eq. (6) is $E = (s - M^2c^2)/2M$ calculated in the reference channel, equal to E_{cm} above. In each channel with masses m_p, m_t and sum M, the wave number is from $k_\alpha^2 = (s - M^2c^2)(s - (m_p - m_t)^2c^2)c^2/(4s(\hbar c)^2)$, and the relative velocity fraction of c, $\beta_\alpha = \sqrt{E_p^2 + 2m_p c^2 E_p}/(E_p + m_p c^2)$, is used for η_α.

2.5 Boundary conditions

The boundary constants B_α above may be set to any constant in each channel, and the same scattering predictions will be obtained after re-adjusting the R-matrix parameters. The B_α must be energy-independent for the general R-matrix derivation to work, otherwise the combination $T_\alpha(R_\alpha) + \hat{B}_\alpha$ would not be Hermitian on the domain $[0, a]$ and the eigen-solutions $\Phi_\alpha^p(R_\alpha)$ would not form an orthonormal set.

Commonly we use $B_\alpha = -\ell_\alpha$ for channel angular momentum ℓ_α, since that is the approximate low-energy behavior of $aH_\alpha^{+\prime}(ka)/H_\alpha(ka)$ and then $\mathbf{L} \simeq 0$, so (as seen from eq. (13)) the S matrix pole will be close in energy to the R-matrix pole for that state. This is very convenient when matching R-matrix energies e_p with observed narrow peaks in cross-sections. At higher energies, the peaks in the cross-section will in general shift from the pole energies e_p, which is why $S(E)$ of eq. (9) is called the shift function. Another option is to set $B_\alpha = aH_\alpha^{+\prime}(ka)/H_\alpha(ka)$ for a particular energy $E = k^2/2\mu$ of a bound state or a resonance, so then $\Re e\mathbf{L} = 0$ at that energy, and the S and R pole energies will more closely coincide (and be identical for bound states). Unfortunately, however, that can be done at only one energy as B_α is a constant for all energies.

For some years, an *ad hoc* workaround was used to improve the agreement of R-matrix poles and resonance positions. That is to allow the "constants" B_α to *vary* with energy as $B_\alpha = S_\alpha(E)$, though this breaks the general derivation of sect. 2.1. This non-physical short-cut proved to be very convenient, as then the terms $S_\alpha(E) - B_\alpha = 0$ in eq. (7) at *all* energies. Now narrow cross sections peak at almost exactly the pole energies e_p since $\mathbf{L} = i\mathbf{P}/a$ is also small. However, this short-cut is generally incorrect as it breaks orthogonality at different energies. Instead, we now recommend using Brune's "alternative transformation" [20] described in sect. 2.8 below.

2.6 Channel radii

Some codes treat the R-matrix radii $\boldsymbol{a}$ as adjustable parameters. However, since the channel radius $\boldsymbol{a}$ is not an observable quantity, it is hard to interpret the uncertainty of such a variable, so we generally discourage that practice. More often we determine the radius parameter starting from a formula and keep it constant throughout the fitting procedure. Larger radii are needed when it is expected that the underlying Hamiltonian has long-ranged interaction terms, but in R-matrix practice increasing the radii means that the poles for the non-resonant background components become lower in energy and more numerous, and so more difficult to fix.

The radii can easily be varied in different mass channels and in different spin-groups $J\pi$, but there is no exact transformation to convert an R-matrix parameter set from one radius to another. One approximate method is to keep constant the formal widths $\Gamma = 2\gamma^2 P$, while another way would be to keep the "observed widths" or the Brune widths (see below) constant. These methods would have to be checked and verified during the fitting procedure.

Another *ad hoc* procedure that is sometimes used to fit cross sections, is to have *different* radii for evaluating the penetrabilities P_α and for evaluating the hard-sphere phase shifts ϕ_α. In such cases, energy-dependent channel radii have also been used for the hard-sphere phase shifts. In practice, this means that different Coulomb functions are used at different radii for different parts of the calculation (eqs. (8) and (11)). This is a convenient way of shifting systematically the phase shifts of all resonances together, however it should also be discouraged because it breaks the identity between methods using eq. (5) and methods using eq. (13). In this work, we have not used different radii for different parts of the calculation. Although the R-matrix formalism allows different radii to be used for every channel, we have used the same radii for all spin groups corresponding to the same particle pair.

2.7 Unitarity

The expression for the S-matrix $\mathbf{S}$ in terms of a (symmetric and real) standard R-matrix $\mathbf{R}$ satisfies unitarity by default, as can be seen directly from eq. (5). However, the Reich-Moore approximation [21] for eliminated γ-channels yields a complex R-matrix (due to the resonant capture widths appearing as imaginary terms in the denominator

of the reduced R-matrix), after reduction to the particle-channel space. Although the S-matrix corresponding to the reduced R-matrix in the particle channel is now not unitary, the complete S-matrix (that includes the eliminated capture channels) is made unitary by equating the capture cross section to the deviation from unitarity of the Reich-Moore R-matrix in the particle channel space. This prescription has been suggested by Froehner [22], and it has been generalized into manifestly unitary form by Arbanas *et al.* [23]. While the full R-matrix accounts for all channels (including individual capture channels), when the number of capture channels becomes large then the generalized Reich-Moore reduced R-matrix approximation could be used to fit only the *total* capture cross section while preserving unitarity [23]. In general we should try to satisfy unitarity exactly at all energies except when there are known open channels being treated inclusively.

2.8 Equivalent transformations

Brune [20] suggested an "alternative parametrization" of the R-matrix parameters, and showed that it transforms both to and from the standard formulation, so they are exactly physically equivalent. Starting from the standard set $\{e_p, \gamma_{p\alpha}\}$ (in matrix form $\{\boldsymbol{e}, \boldsymbol{\gamma}_\alpha\}$), he constructs the real symmetric and energy (E) dependent matrix

$$\mathbf{A}(E) = \boldsymbol{e} - \sum_\alpha \boldsymbol{\gamma}_\alpha \boldsymbol{\gamma}_\alpha^T \quad (S_\alpha(E) - B_\alpha) \tag{14}$$

of which the eigen-value problem is

$$\mathbf{A}(E)\, \boldsymbol{c}_p = \tilde{e}_p\, \boldsymbol{c}_p \tag{15}$$

where $\tilde{e}_p$ is the p'th eigenvalue and $\boldsymbol{c}_p$ is the corresponding eigenvector (normalized as $\boldsymbol{c}_p^T \boldsymbol{c}_p = 1$). This eigenvalue problem is solved iteratively for each eigen-solution p, by using at each iteration $\mathbf{A}(\tilde{e}_p)$ the most recent estimate for $\tilde{e}_p$. After convergence to $\mathbf{A}(\tilde{e}_p)\boldsymbol{c}_p = \tilde{e}_p \boldsymbol{c}_p$ for each p, we define $\tilde{e}_p$ as the "alternative R-matrix energy" to be used with the new set of reduced width amplitudes $\tilde{\gamma}_{p\alpha} = \boldsymbol{c}_p^T \boldsymbol{\gamma}_\alpha$. These new parameters are invariant under changes of boundary constants B_α, and if $B_\alpha = S_\alpha(e_p)$ we would have also $\tilde{\gamma}_{p\alpha} = \gamma_{p\alpha}$. Brune describes in sect. III.B of [20] how to transform back to the standard parameter set. In his sect. IV.A, he also shows how these parameters may be used, via the level-matrix formulation, to obtain the scattering S matrix without having to use that back translation.

This reformulation of R-matrix parameters (which we call the "Brune basis") is both very convenient and completely consistent with the standard theory of Lane and Thomas [18], with no *ad hoc* alterations. The Brune energies $\tilde{e}_p$ are now very close to the experimental energies of bound states or resonances, and that is very useful if these are known from mass measurements or other independent experiments.

3 R-matrix codes

3.1 Capabilities of codes

An inter-comparison of the capabilities of the R-matrix codes AMUR, AZURE2, EDA, FRESCOX, GECCCOS, SAMMY and CONRAD is presented in this section. As the codes AMUR, AZURE2, EDA, FRESCOX, GECCCOS, SAMMY, and CONRAD were developed initially for the solution of different problems, each one has its particular features, strengths and weaknesses. Specifics of each code are presented separately in the following while a summary is given in table 1.

AMUR. The AMUR code [24] was developed at the Japan Atomic Energy Agency (JAEA) for the evaluation of cross-sections in the resolved resonance energy region. The code is based on the Wigner-Eisenbud formalism [25] except for the γ-ray channels which are calculated using the Reich-Moore approximation [21]. To facilitate continuous management and further development, the code is based on object-oriented programming (assembly of a number of classes developed using the C++ programming language). The resonance parameters and their covariance matrix are deduced from the experimental observables such as cross-sections, differential cross-sections and analyzing powers through the Kalman filtering method [26]. In addition to the resonance parameters, the experimental parameters (that are involved in the simulation of the experimental conditions) can be estimated within the same framework. Energy resolution, Doppler broadening and renormalization can be considered in the present version of the AMUR code. An example of such an analysis for the ^{17}O compound system where the experimental $n + {}^{16}$O and the $\alpha + {}^{13}$C reaction cross-sections are simultaneously fitted is given in ref. [24].

AZURE2. The original AZURE code (FORTRAN) was developed through a Joint Institute for Nuclear Astrophysics (National Science Foundation Physics Frontier Center) collaboration lead by Azuma [27]. The code was designed for the analysis of charged-particle induced reactions at low energies, with particular emphasis on capture reactions. The AZURE2 code [28] was developed by Uberseder in order to increase the capability of the original code, including a more friendly user interface, a modern programing language (C++), and the ability to perform multiple entrance channel calculations. While AZURE2 is generally applicable to all reaction types, it was tested heavily and customized to analyze the reaction $^{12}\mathrm{C}(\alpha,\gamma)^{16}\mathrm{O}$ [29]. It can calculate and fit to data for unpolarized differential cross sections, angle integrated cross sections, phase shifts, β-delayed particle emission spectra, and angle integrated total capture cross sections. The open source is available at `azure.nd.edu`.

While AZURE2 has the option to make calculations and perform fits using the standard R-matrix parameterization of Lane and Thomas [18], the default and preferred parameterization is that of Brune [20]. For this exercise, the code was modified to use custom boundary conditions B_α when using the standard R-matrix parameterization.

Table 1. Summary of R-matrix codes specifications.

Feature	EDA	AZURE2	AMUR	FRESCOX	SAMMY	CONRAD	GECCCOS
R-matrix	Full	Full	Limited (for γ's)	Full	SLBW, MLBW, RM, Full[a]	SLBW, MLBW, RM, Full[a]	Full
Derivatives	Analytic	Numerical	Numerical	Numerical	Analytical ($T = 0\,\mathrm{K}$) Numerical[b]	Analytic	Numerical
Reference frame	Lab/CM	In Lab, Out CM	Lab/CM	Lab/CM	Lab/CM	Lab/CM	Lab/CM
(Non)Relativistic kinematics	R + NR	NR	NR	R, NR	N-R	R, NR	NR
Channel Radii	Varied	Varied	Fitted (option)	Fixed	Varied	Varied	Fixed/Varied
Photons	In/Out	Out	Out	In/Out	Out	Out	
Observables: E, θ cross sections	All	All	All	All	All	All	All
Observables: polarization T_{kq}	All	No	Yes	All	No[c]	No	No (planned)
Inverse reactions	Yes	Yes	Yes	Yes	Yes	Yes	Yes
Decay gammas	Post-processing	No	No	Post-processing	No	No	No
Isobaric reactions simultaneously	Yes	No	No	No	No	No	No
Doppler broadening	No	No	Yes	No	Yes	Yes	No
Resolution broadening	Yes	Yes	Yes	No	Yes	Yes	No
Normalization	Yes	Yes	Yes	yes	Yes	Yes	Yes
Background subtraction	No	No	Yes	No	Yes	Yes	No
Background R-matrix terms	E-dependent	Distant poles	Distant poles	Distant poles	Yes	No (planned)	Yes
Sample-size corrections	No	Yes	No	No	Yes	Yes	No
Close-geometry Q-corrections	No	Yes	No	No	Yes	No	No
Fitting procedure	LSQ	MINUIT2	KALMAN	MINUIT1	Bayesian (GLS)	Bayesian (GLS)	DAKOTA [41]
Multiple data sets S: Simultaneously	S	S	S	S	S	S	S
Uses data covariances	No	No	Yes	No	Yes	Yes	No[d]
Prior parameter covariances	Yes	No	Yes	No	Yes	Yes	No[d]
Data covariances (MF 32)	No	No	No	No	Yes	Yes	No
Brune parameter output	No (planned)	Yes	No	No	No (planned)	No (planned)	No (planned)
ENDF-6 format output	Yes	No	Yes	No	Yes	Yes	No[d]
ENDF-6 input	No	No	No	No	Yes	Yes	No
Code language	F77	C++	C++	F90	F77[e]	C++	F03
Export controlled	Yes	No	Yes	No	RSICC[f]	Yes	No
Documentation	No	Yes	No	Yes	Online	No	No[g]
Parallelized	No	Yes	Yes	No	No	Yes	Yes
Interactive fitting	Yes	No	No	Yes	Yes	Yes	No
PPP modification			logarithmic fit	No	Experimental covariances	Marginalization	

[a] Full R-matrix in SAMMY and CONRAD is achieved by treating γ-channels as reaction channels.

[b] Analytic derivatives of cross sections at $T = 0\,\mathrm{K}$, numerical derivatives of Doppler-broadened and resolution-broadened cross sections.

[c] SAMINT links to IBE.

[d] provides the input for a separate Bayesian evaluation code, which delivers all the mean values and covariances of considered observables.

[e] SAMMY modernization in progress: the SAMRML code has been modernized into C++.

[f] SAMMY may have its export-controlled classification removed.

[g] Source code documentation available, manual in preparation.

Special care must be taken for accurate calculation of the Coulomb functions at low energies. AZURE2 provides two options for calculation: the GNU scientific library [30] and those of Michel [31]. The GSL routines are much faster computationally, but are less accurate than those of [31] over certain energy ranges. The Whittaker functions of GSL are used exclusively. See sect. 5.2 for further discussion.

For fitting, the code uses the package MINUIT2 [32] to search for the minimum in χ^2. The χ^2 function is given as [33]

$$\chi^2 = \sum_i \left(\sum_j \frac{(f(x_{i,j}) - n_i y_{i,j})^2}{(n_i \sigma_{i,j})^2} + \frac{((1-n_i)/n_i)^2}{\delta^2_{exp,i}} \right), \tag{16}$$

where $f(x_{i,j})$ are the R-matrix calculated values and $y_{i,j}$ are the experimental data points with corresponding point-to-point uncertainties $\sigma_{i,j}$. The sums run over the number of data points j in a particular data set i. The second term in eq. (16) takes into account a constant renormalization factor n_i that is constrained by a systematic uncertainty $\delta^2_{exp,i}$ for each data set.

EDA. The Energy-Dependent Analysis code (EDA) was originated at Los Alamos National Laboratory in the early 1970s by Dodder and Witte, with subsequent contributions by Hale and Sierk. It was envisioned by Don Dodder to be a completely general R-matrix program, with no restrictions on the types of particles (neutral and charged, massless and massive) considered. Therefore the default kinematics are relativistic, with an option to use non-relativistic kinematics. The code implements the full multi-level, multichannel R-matrix treatment of Lane and Thomas [18], and calculates scattering observables using the general operator formalism of Wolfenstein [34], which is based on the spin-space matrix elements of the transition operator, the Wolfenstein M-matrix. This allows for the inclusion of polarization observables in addition to cross sections in the experimental data base. The treatment of photon channels differs from that given in Lane and Thomas, and is based on the scattering formalism for classical electromagnetic radiation given by Newton (see [35], chapt. 2).

The χ^2 expression minimized by EDA is essentially the same as that given above for AZURE2, but normalization parameters are the reciprocals of those used by AZURE2. The minimization is accomplished by using a modified variable metric search method, with analytic first derivatives of χ^2. Besides normalizations, the code allows some other forms of data correction, including resolution folding and automated energy shifting. Correlations among the input experimental data are not taken into account, other than those induced by overall normalization factors. The parameter covariance matrix comes out of the search algorithm, which builds up the Hessian (inverse second-derivative) matrix using a rank-one iterative method that is quadratically convergent.

FRESCOX. The code FRESCO was developed at Daresbury Laboratory, UK, by Thompson for solving coupled-channels scattering problems using FORTRAN, and summarized in the paper [36]. At the University of Surrey it was extended to include searches by χ^2 minimization, and to use R-matrix inputs in place of Hamiltonian specifications. The version FRESCO is available online [37] and at Github [38]. Since 2006 a more advanced version FRESCOX has been developed at LLNL, enabling more flexible R-matrix specifications for LS couplings, Reich-Moore approximations, and Brune-basis parameters [20].

GECCCOS. The GECCCOS code is a coupled-channel program developed at TU Wien by Srdinko and Leeb, which is dedicated to calculations of reactions of light nuclear systems. Especially, it is envisaged for reaction calculations covering the whole resonance range up to energies at which the nuclear statistical model is applicable. Thus together with the code TALYS [39] it provides the necessary tools and output for a consistent Bayesian evaluation of nuclear reactions. In order to guarantee a smooth transition between the resonance regime and statistical model calculations, an R-matrix representation of the coupled-channel potential model needs to be developed. Consequently, a key feature of GECCCOS is that it combines the calculable R-matrix with the phenomenological R-matrix approach, *e.g.* using background poles associated with a potential model. For the calculable R-matrix the Lagrange mesh technique introduced by Baye and Descouvemont [19] is implemented to solve the coupled-channel equations. The Coulomb wave functions are obtained from the COULCC routines by Thompson and Barnett [40]. Since they allow complex arguments, open and closed channels for neutral and charged particle reactions can be treated with the same routines. The adjustment of the phenomenological R-matrix as well as of the potential parameters is performed via the DAKOTA package [41] which allows GECCCOS to apply conceptually different optimization procedures such as gradient methods, evolutionary algorithms and global Monte Carlo based methods.

The code is still under development and due to its modular structure the implementation of new features is manageable with reasonable effort. In the near future it is planned to include the Brune parametrization and the handling of polarization data.

SAMMY. The Oak Ridge National Laboratory (ORNL) legacy code SAMMY [42] is used worldwide to evaluate differential cross-section data for nuclear reactions in the resolved and unresolved resonance energy ranges induced by incoming neutrons, protons, and α-particles. SAMMY updates phenomenological non-relativistic R-matrix resonance parameters via the Newton-Raphson iterative minimization of the generalized χ^2-function to yield optimal posterior resonance parameter values, their covariance matrix, and the corresponding evaluated nuclear data and covariance matrix. Although the SAMMY code has been primarily conceived for evaluations of heavy and medium mass nuclides for which Reich-Moore approximation is

necessary due to the large number of capture channels, the code is also capable of treating individual capture channels without the Reich-Moore approximation. Unitarity is enforced by design in SAMMY's implementation of the Reich-Moore approximation, as explained in sect. 2.7. SAMMY accounts for various experimental effects that are custom tailored to several leading measurement facilities and detectors. Over several decades, SAMMY has become established as an important tool for nuclear data resonance parameter evaluations disseminated via the US Evaluated Nuclear Data File (ENDF) for simulations of nuclear systems by neutron transport code systems such as SCALE.

The R-matrix algorithm implemented in the released version of the SAMMY code [42] was designed to use the energy-dependent boundary condition $B_\alpha = S_\alpha$. This choice was motivated by the limited number of partial waves, typically only s-wave, used to evaluate neutron resonance parameters for heavy (fissile) nuclei that usually do not account for threshold reaction channels in the analyzed resolved resonance region. In view of the requirements for the analysis of the ^{7}Be compound system, corrections to the SAMMY code algorithm were made, both in the computation of the R-matrix elements and in the calculation of the shift functions for negative energies, to take into account the boundary condition $B_\alpha = -\ell_\alpha$ for reaction channels with energy threshold. These updates will be included in the SAMMY-8.2 release also to guarantee full consistency in the conversion algorithm between "formal" and "alternative" R-matrix parameters developed by Brune [20].

CONRAD. The CONRAD [43] code is developed at CEA Cadarache for the evaluation of nuclear reactions relevant to nuclear reactor applications, in particular for the production of nuclear data from 0 to 20 MeV incident neutron energy. The fast energy region is treated by combining ECIS [44] and TALYS [39] codes and adjusting optical model and statistical parameters whereas for the resolved resonance region modules specific to CONRAD are used. In this latter domain, the original capabilities of the code that were oriented to neutron-induced reactions have recently been extended to treat charged projectiles and ejectiles. These new capabilities benefit from pre-existing features of the code that were developed for the analysis of microscopic experiments (Doppler broadening, resolution function, sample characteristics, etc.). The code can also update the resonance parameters from integral feedback from reactor physics experiments. The data assimilation is performed by using the GLS formalism (Newton-Raphson iterative minimization) and Analytical and/or Monte Carlo Marginalization [45].

As mentioned for the SAMMY code, CONRAD was also developed with the adopted boundary condition of $B_\alpha = S_\alpha$ as this was satisfactory for dealing with neutron-induced reactions on actinides. For the present work on ^{7}Be the code was updated to allow for user-provided boundary conditions. The simplified expressions [46] for the computation of the penetration factor P_α, the shift factor S_α and hard-sphere phase shift ϕ_α that hold for neutron channels had to be replaced by algorithms that compute them directly from Coulomb wave functions [31]. As the recurrence relations between these coefficients still holds for charged-particles channels [18], the extra computational cost of using Coulomb wave functions is limited. Finally, the extension of CONRAD to treat charged-particles channels also required the inclusion of the Rutherford scattering amplitude and the interference term for the angular distribution analysis, which was not needed for neutron reactions.

4 Interchanging input resonance parameters: The Ferdinand code

In order to compare evaluations from different codes, we want to translate resonance parameters (E_p, $\gamma_{p\alpha}$) between the file formats of the codes, and also convert to the Brune basis parameters ($\tilde{E}_p$, $\tilde{\gamma}_{p\alpha}$) of [20], which have the advantage of being independent of the boundary conditions. One of us (IT) therefore wrote the Python code FERDINAND using the FUDGE library [47], with the GNDS format [48] as the internal storage structure. This code translates from GNDS, ENDF, FRESCOX, AZURE2, AMUR, and EDA formats, and writes GNDS, ENDF, AZURE2, EDA, FRESCOX, HYRMA and LaTex format files. It optionally performs Barker transformations [49] to the Brune basis, and allows the user to specify any energy-independent boundary conditions B_α in the reverse Brune transformation. It can remove or add Reich-Moore and other channels, remove poles outside energy limits, change the elastic channel, convert between amplitudes and formal widths, and call FRESCOX for point-wise reconstruction of energy and/or angular distributions. We have not attempted methods for changing R-matrix radii.

5 Exercise: Comparison of R-matrix algorithms

The main objective of this work was to verify that the different R-matrix codes under consideration calculate the same cross sections for a given set of input parameters. The level of consistency between the different codes has been deemed a necessary first step for future evaluation work. Only charged-particle channels were considered in this comparison for simplicity. Break-up channels are not treated by the R-matrix codes considered herein. On the other hand, photon channels are treated rather differently by the different codes, with some considering them explicitly wheres others such as AMUR, SAMMY, and CONRAD adopting the Reich-Moore approximation. Moreover, most of the codes do not yet include the important secondary photon emission channel either (such as $(\mathrm{p}, \mathrm{p}'\gamma)$). The comparison of the codes with respect to the above mentioned items will be the subject of a second exercise that will focus on the evaluation of the light system ^{7}Be.

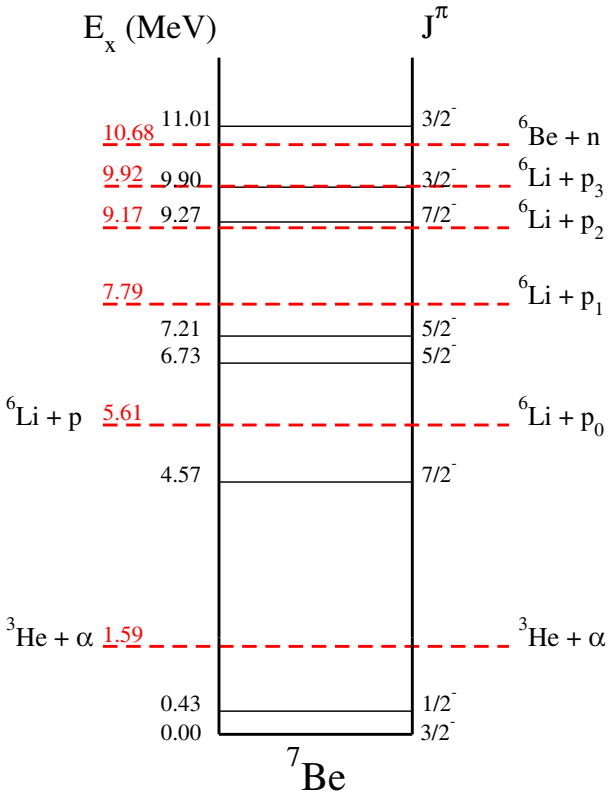

Fig. 1. Level diagram of ^{7}Be. The low mass nucleus has only two bound states, the ground state and the level at $E_x = 0.429\,\text{MeV}$.

5.1 Description

The goal of this exercise was to compare the R-matrix algorithms implemented in the codes. All contributing code developers were asked to calculate cross sections for a light system, namely ^{7}Be, which was chosen due to its relatively simple level scheme at low energies below the particle breakup threshold, as can be seen in fig. 1. The calculations were limited to excitation energies up to $E_x = 8\,\text{MeV}$ so as to include only two particle partitions, $\alpha + {}^3\text{He}$, and $p + {}^6\text{Li}$ and avoid the complication of particle-breakup channels while photon channels were also omitted. Masses and Q-values as well as fundamental constants were set to the values proposed in the ENDF-6 manual [46] and are given in table 2.

At the energies considered, only the following particle channels are open: $\alpha({}^3\text{He}, {}^3\text{He}_0)\alpha$, ${}^6\text{Li}(p, \alpha_0){}^3\text{He}$, ${}^6\text{Li}(p, p_0){}^6\text{Li}$, and their inverse.

The resonance parameters (pole energies and reduced width amplitudes) are given in table 3 for the poles that have non-zero reduced width amplitudes in at least one channel. Additional poles, with reduced width amplitudes that were set to zero for all channels, were required by some codes for angular momentum and spin conservation selection.

A set of data was considered as a convenient way to establish an energy and angle grid for the calculations. Cross sections were calculated in the frame of reference

Table 2. Particle pair information for ^{7}Be compound system. Atomic asses are in amu (taken from AME2016), separation and excitation energies in MeV, and channel radii in fm. Constants are taken from NIST and are the same as those used in ENDF6. Note: Channel radii are calculated using integer masses.

particle pair 1		
particle 1:	^{4}He	
	$J^\pi =$	0^+
	$M =$	4.002603
	$Z =$	2
particle 2:	^{3}He	
	$J^\pi =$	$\frac{1}{2}^+$
	$M =$	3.016029
	$Z =$	2
particle pair 2		
particle 1:	^{1}H	
	$J^\pi =$	$\frac{1}{2}^+$
	$M =$	1.007825
	$Z =$	1
particle 2:	^{6}Li	
	$J^\pi =$	1^+
	$M =$	6.015122
	$Z =$	3
constants		
$a_c =$	$1.4\ (A_1^{1/3} + A_2^{1/3})$	fm
Q-value $[{}^6\text{Li}(p,\alpha)] =$	4.01972	MeV
$\hbar c =$	197.3269788	MeV fm
$\mu =$	931.4940954	MeV/c^2
$\alpha_f^{-1} =$	137.035999139	

of the existing data (for $\alpha({}^3\text{He}, {}^3\text{He}_0)\alpha$, ${}^6\text{Li}(p,\alpha){}^3\text{He}$, and ${}^6\text{Li}(p,p){}^6\text{Li}$ in the laboratory frame and ${}^3\text{He}(\alpha,p){}^6\text{Li}$ in the center-of-mass frame) and included excitation functions at given angles as well as angular distributions at given energies. A list of measured excitation functions and angular distributions is given in table 4. The listed data sets were extracted from EXFOR [50] and sent to all contributors by deBoer except for those of [51] ${}^3\text{He}(\alpha,p){}^6\text{Li}$, which were taken from the EDA (Los Alamos) database.

The calculations were performed using the boundary conditions $B = -\ell$ (orbital angular momentum) and maximum orbital angular momentum needed to produce all channels up to $\ell = 4$ for the ${}^3\text{He} + \alpha$ and $\ell = 1$ for ${}^6\text{Li} + p$ for $J^\pi = 9/2^-$ (see note above). Channel radii were determined as $a_\alpha = 1.4$ [fm] $(A_1^{1/3} + A_2^{1/3})$ ($a_\alpha({}^3\text{He} + \alpha) = 4.241511\,\text{fm}$, $a_\alpha({}^6\text{Li} + p) = 3.943969\,\text{fm}$), and were the same for all channels within a particle pair.

Table 3. R-matrix parameters in the $B = -\ell$ basis. Pole energies in the center-of-mass frame of the elastic channel. Reduced width amplitudes are given in $\mathrm{MeV}^{1/2}$.

$J^\pi = 1.5^-$				
E	^{1}H+^{6}Li	^{1}H+^{6}Li	^{1}H+^{6}Li	^{4}He+^{3}He
(MeV)	ℓS: 1, 1/2	ℓS: 1, 3/2	ℓS: 3, 3/2	ℓS: 1, 1/2
−1.586097	−1.34077	−0.41816	0.00000	1.05725
$J^\pi = 2.5^-$				
E	^{1}H+^{6}Li	^{1}H+^{6}Li	^{4}He+^{3}He	
(MeV)	ℓS: 1, 3/2	ℓS: 3, 1/2	ℓS: 3, 1/2	
5.746671	0.94880	0.00000	0.18770	
7.088367	−0.34947	0.00000	1.18381	
$J^\pi = 3.5^-$				
E	^{1}H+^{6}Li	^{1}H+^{6}Li	^{1}H+^{6}Li	^{4}He+^{3}He
(MeV)	ℓS: 3, 1/2	ℓS: 3, 3/2	ℓS: 5, 3/2	ℓS: 3, 1/2
3.483949	0.00000	0.00000	0.00000	0.79362

Table 4. Summary of data including EXFOR entry numbers. Thanks to Mark Paris and Gerry Hale for giving more detailed (α, p_0) cross section data for the experiment reported in ref. [51].

Ref.	Data type	File name	Source (EXFOR)
[52]	^{3}He$(\alpha,\alpha)^3$He, $\frac{\mathrm{d}\sigma}{\mathrm{d}\Omega}$	Barnard_aa.dat	A1269002
[53]	^{3}He$(\alpha,\alpha)^3$He, $\frac{\mathrm{d}\sigma}{\mathrm{d}\Omega}$	Tombrello_aa.dat	A1295002
[54]	^{6}Li$(p,p)^6$Li, $\frac{\mathrm{d}\sigma}{\mathrm{d}\Omega}$	McCray_pp.dat	A1410002
[55]	^{6}Li$(p,\alpha)^3$He, $\frac{\mathrm{d}\sigma}{\mathrm{d}\Omega}$	Elwyn_pa.dat	F0012002, F0012003

Here A_1 and A_2 are the *integer* mass numbers, not reduced atomic masses. Only charged-particle channels were considered.

5.2 Coulomb functions

The Coulomb functions F_ℓ, G_ℓ and/or $H_\ell^\pm$ need to be accurately calculated in order for the predicted cross-sections to follow correctly from the R-matrix parameters. The functions depend on partial wave ℓ, radius $\rho = kR$, and Sommerfeld parameter η as $H_\ell^\pm(\rho,\eta) = G_\ell(\rho,\eta) \pm iF_\ell(\rho,\eta)$. As an exercise, we extracted from each collaborator's code the three Coulomb-dependent functions, penetrability P, shift function S, and hard-sphere phase shift ϕ of eqs. (8), (9), and (11) respectively, for partial waves ℓ from 0 through 9 at energies −5 to +20 MeV in the two mass partitions of the joint exercise. These values were compared with those from the standard routine COULCC [40, version 36], and in fig. 2 we plot the maximum differences over all energies (except within 50 keV of thresholds). For S and P we also plot the results from $S + iP = \rho H^{+\prime}/H^+$ directly evaluated by the complex continued fraction CF2 [40].

Figure 2 shows that all codes agree with accuracies better than 10^{-4}, except for AMUR which is sometimes differing by more than this.

5.3 Results

The results of the exercise were compared by taking the ratio of each code's calculated cross sections with respect to those from the code AZURE2 as shown in figs. 3, 4, 5, and 6. Throughout this section, when the level of consistency between calculations is discussed, it refers to this ratio. As a compromise between practicality and accuracy, a threshold of ±0.5% from unity has been chosen as the criterion for acceptable agreement between the codes.

In general this goal was achieved, but in a few cases larger deviations were observed. These larger deviations appeared exclusively in the calculations of the cross sections of the ^{3}He$(\alpha,\alpha)^3$He reaction and were usually either near the central energy of sharp resonances or at large scattering angles. A high level of consistency was achieved between AZURE2 and FRESCOX, usually to better than 0.01%, for all calculations.

On the other hand, the constancy between the $^6\mathrm{Li} + p$ calculations was found to nearly always be much better than the target level of consistency. Note that the scale for the ratio axis in figs. 3 and 4 runs from 0.995 to 1.005, those of figs. 5 and 6 have smaller scales. When these smaller scales are used some "choppiness" can appear. This is not a real effect but the result write out precision.

(α,α) channel. By far the largest inconsistencies between different calculations were observed for the α-scattering data sets. For the energy/angle grid of the data of ref. [52] (see fig. 3), significant differences were observed near the sharp $7/2^-$ resonance near 7 MeV. The consistency between AZURE2 and FRESCOX was maintained and nearly the same level of consistency was also obtained for CONRAD and AMUR. The calculations with SAMMY and EDA showed larger deviations but still remained better than 0.5% except at a few angles very close to the resonance energy.

For the higher energy data of ref. [53], the largest discrepancies were observed for the entire exercise as shown in fig. 4. Still, most deviations remained below the 0.5% level except at the two largest angles. A high level of consistency was obtained between AZURE2, FRESCOX, and AMUR, but much larger deviations were observed for EDA, GECCCOS, CONRAD, and SAMMY.

(p,p) channel. For the energies and angles of the proton scattering data of ref. [54] excellent agreement was obtained for all data sets, with ratios shown in fig. 5. The largest deviations were observed for SAMMY and GECCCOS, but they are still well below the 0.5% level.

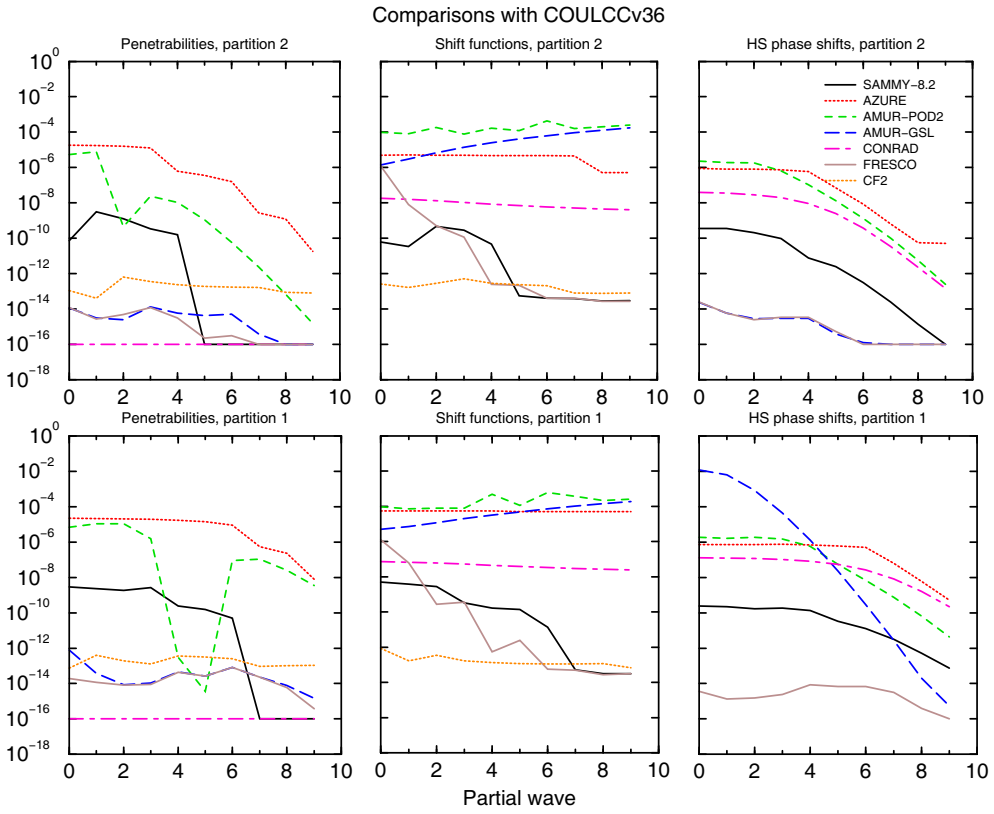

Fig. 2. Differences of P (center), S (middle) and ϕ (right), in rows for each mass partition, with the results from COULCC ([40], version 36). The values are the maximum differences over all energies, except within 50 keV of threshold.

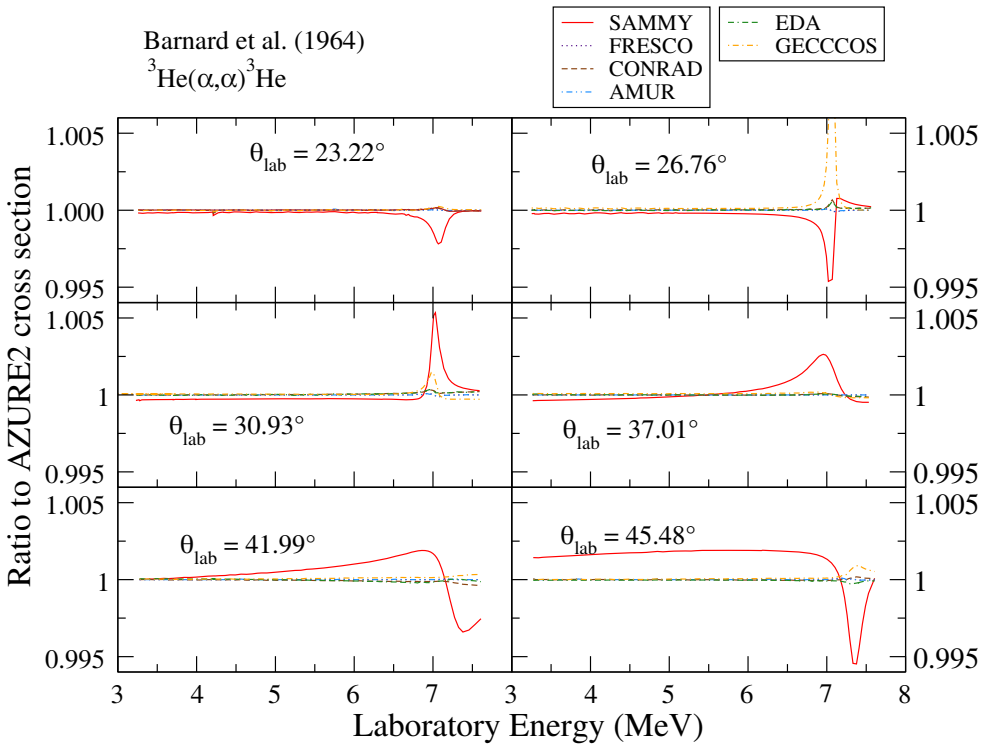

Fig. 3. Comparison of calculations to AZURE2 results for the $^3\mathrm{He}(\alpha,\alpha)^3\mathrm{He}$ reaction using the energies and angles of the [52] data. Here the vertical axis is scaled to a uniform 1%.

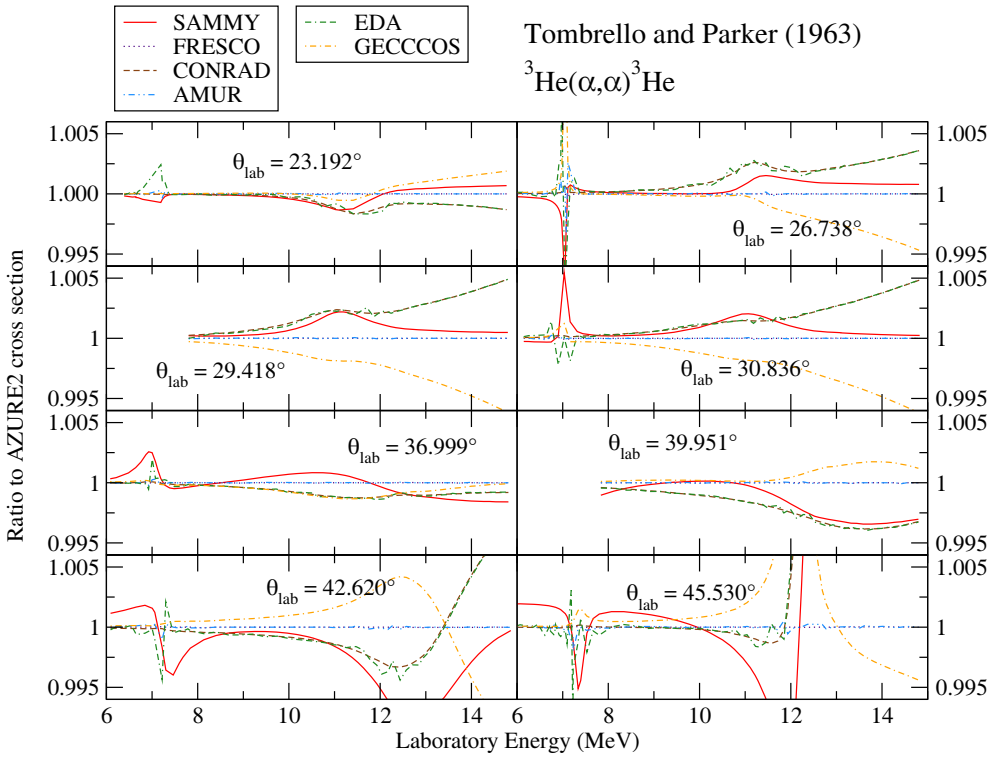

Fig. 4. Comparison of calculations to AZURE2 results for the $^3\mathrm{He}(\alpha,\alpha)^3\mathrm{He}$ reaction using the energies and angles of the [53] data. Here the vertical axis is scaled to a uniform 1%.

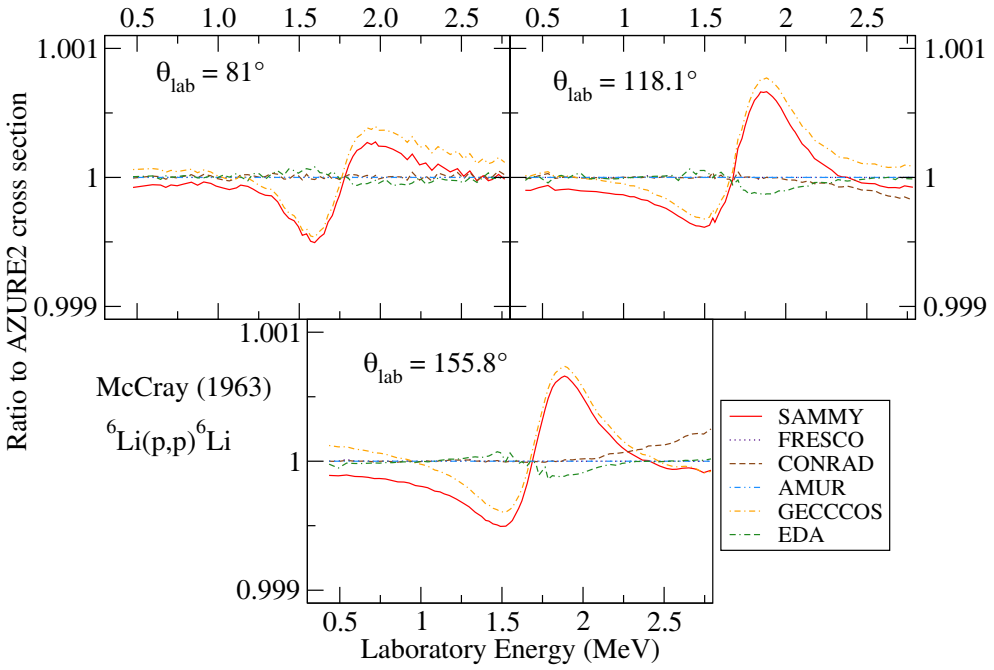

Fig. 5. Comparison of calculations to AZURE2 results for the $^6\mathrm{Li}(p,p)^6\mathrm{Li}$ reaction using the energies and angles of the ref. [54] data. Here the vertical axis has been scaled to a uniform 0.2%.

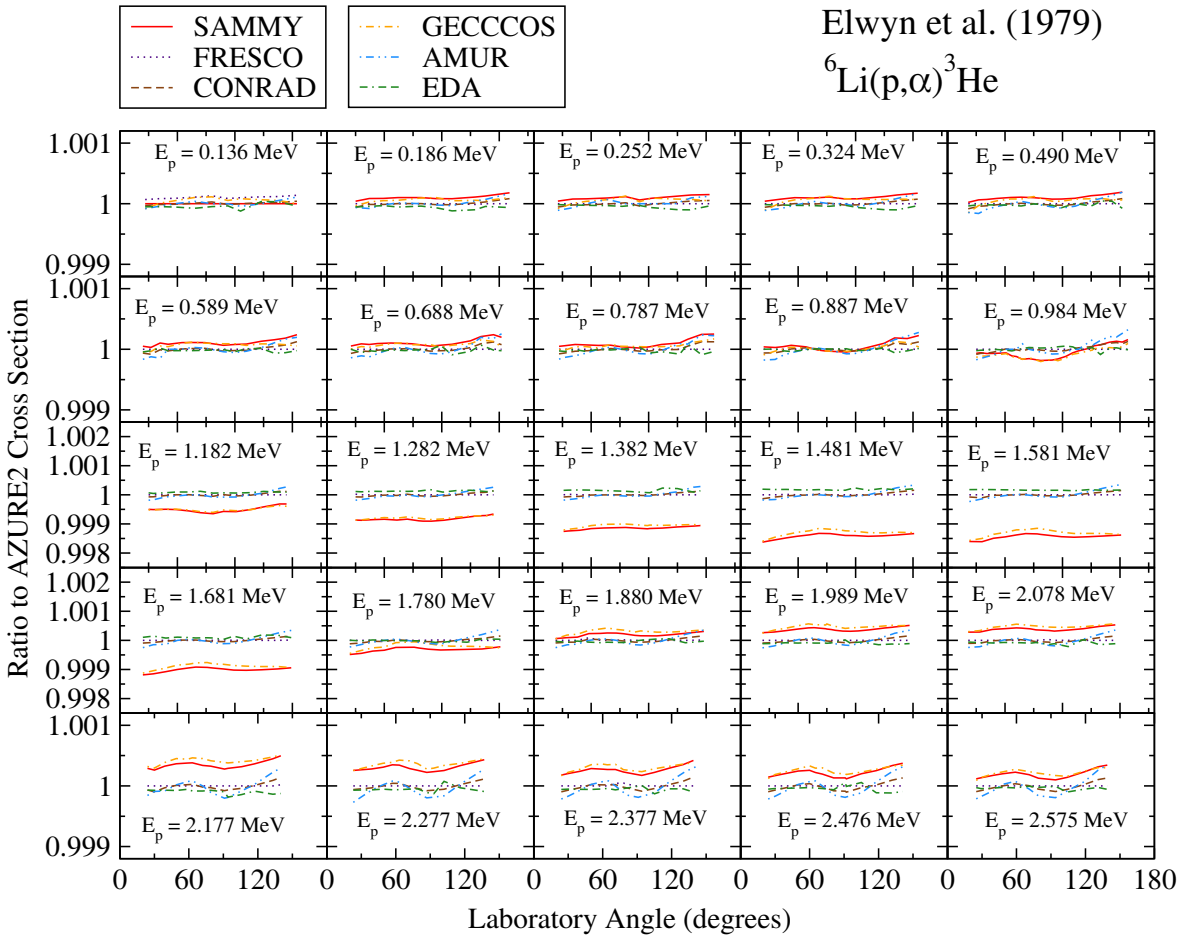

Fig. 6. Comparison of calculations to AZURE2 results for the ^{6}Li$(p,\alpha)^3$He reaction using the energies and angles of the ref. [55] data. Note that for the intermediate energies the vertical axis scale is 0.4%, while for the others the scale is 0.2%.

(p,α) *channel*. Similar to the proton scattering, the comparison calculations at the energies and angles of the (p,α) data of ref. [55] were found to produce very consistent results across all of the codes. Again, the largest deviations were those of SAMMY and GECCCOS, but these were always less than 0.2% from unity. Ratios are shown in fig. 6.

6 Conclusion

An inter-comparison of the capabilities of the R-matrix codes AMUR, AZURE2, EDA, FRESCOX, SAMMY and CONRAD was performed. As these codes were developed initially for the solution of different problems, each one has its particular features, strengths and weaknesses.

A necessary condition to perform useful comparisons of R-matrix calculations was the interchangeability and translatability of R-matrix input and output parameters between the various codes. The Ferdinand code to convert R-matrix fits between several formats, including ENDF, GND, and the various formats used for the input and output of the above-mentioned R-matrix codes was developed.

The ability of the different codes to calculate charged-particle reaction cross sections in the resolved resonance region was verified by means of a joint exercise. The exercise involved calculating cross sections for charged-particle elastic scattering and charge-exchange reactions leading to the compound system ^{7}Be in a given energy region and using well-defined input parameters. Only charged-particle channels were considered avoiding the complications of break-up channels while photon channels were omitted.

The results revealed that using different kinematics or different ways of calculating the Coulomb functions as well as other approximations such as excluding closed channels, can have a impact on the R-matrix calculations.

On the whole, all the codes agreed to within 0.1–0.3% which is far below the uncertainties of the existing experimental data in this low-energy region. In a next step, the codes will be used to evaluate the light system ^{7}Be so as to compare the treatment of i) other channels such as photon and break-up channels, and ii) uncertainties and their correlations.

This work was performed under an IAEA project on R-matrix Codes for Charged-Particle Reactions in the Resolved-Resonance Region. RJD would like to recognize support from the Notre Dame Center for Research Computing and funding by the National Science Foundation through Grant No. Phys-0758100, and the Joint Institute for Nuclear Astrophysics through Grant No. Phys-0822648. The work of IJT was performed under the auspices of the U.S. Department of Energy by Lawrence Livermore National Laboratory under Contract DE-AC52-07NA27344. ORNL work was supported by U.S. Department of Energy (DOE), Nuclear Criticality Safety Program (NCSP) funded and managed by National Nuclear Security Administration (NNSA) for DOE.

Data Availability Statement This manuscript has no associated data or the data will not be deposited. [Authors' comment: All data generated during this study are contained in this published article.]

Publisher's Note The EPJ Publishers remain neutral with regard to jurisdictional claims in published maps and institutional affiliations.

References

1. Technical Report IAEA TECDOC-1780, International Atomic Energy Agency, Vienna, Austria (2015).
2. Technical Report IAEA TECDOC-1822, International Atomic Energy Agency, Vienna, Austria (2017).
3. *Ion beam analysis nuclear data library*, `http://www-nds.iaea.org/ibandl`, IAEA, Vienna, Austria.
4. P. Dimitriou, V. Semkova, V. Zerkin, EPJ Web of Conferences **146**, 09014 (2017).
5. A. Gurbich, Nucl. Instrum. Methods Phys. Res. B **371**, 27 (2016).
6. S. Simakov, Q.Y. van den Berg, Nucl. Data Sheets **139**, 190 (2017).
7. C. Angulo, M. Arnould, M. Rayet, P. Descouvemont, D. Baye, C. Leclercq-Willain, A. Coc, S. Barhoumi, P. Aguer, C. Rolfs *et al.*, Nucl. Phys. A **656**, 3 (1999).
8. Y. Xu, K. Takahashi, S. Goriely, M. Arnould, M. Ohta, H. Utsunomiya, Nucl. Phys. A **918**, 61 (2013).
9. R.H. Cyburt, A.M. Amthor, R. Ferguson, Z. Meisel, K. Smith, S. Warren, A. Heger, R.D. Hoffman, T. Rauscher, A. Sakharuk *et al.*, Astrophys. J. Suppl. **189**, 240 (2010).
10. Y. Xu, S. Goriely, A. Jorissen, G.L. Chen, M. Arnould, Astron. Astrophys. **549**, A106 (2013).
11. I. Dillmann, R. Plag, F. Käppeler, T. Rauscher, *KADoNiS v0.3 - The third update of the "Karlsruhe Astrophysical Database of Nucleosynthesis in Stars"* (2010).
12. Computational Infrastructure for Nuclear Astrophysics, `http://nucastrodata.org/`.
13. P. Dimitriou, R.J. deBoer, S. Kunieda, H. Leeb, M. Paris, T. Srdinko, I.J. Thompson, Technical Report INDC(NDS)-0703, International Atomic Energy Agency, Vienna, Austria (2016) `https://www-nds.iaea.org/publications/indc/indc-nds-0703.pdf`.
14. H. Leeb, P. Dimitriou, I.J. Thompson, Technical Report INDC(NDS)-0726, International Atomic Energy Agency, Vienna, Austria (2017) `https://www-nds.iaea.org/publications/indc/indc-nds-0726.pdf`.
15. H. Leeb, P. Dimitriou, I.J. Thompson, Technical Report INDC(NDS)-0737, International Atomic Energy Agency, Vienna, Austria (2017) `https://www-nds.iaea.org/publications/indc/indc-nds-0737.pdf`.
16. H. Leeb, P. Dimitriou, I.J. Thompson, Technical Report INDC(NDS)-0767, International Atomic Energy Agency, Vienna, Austria (2018) `https://www-nds.iaea.org/publications/indc/indc-nds-0767.pdf`.
17. Technical Report STI/PUB/1291, International Atomic Energy Agency, Vienna, Austria (2007).
18. A.M. Lane, R.G. Thomas, Rev. Mod. Phys. **30**, 257 (1958).
19. P. Descouvemont, D. Baye, Rep. Prog. Phys. **73**, 036301 (2010).
20. C.R. Brune, Phys. Rev. C **66**, 044611 (2002).
21. C.W. Reich, M.S. Moore, Phys. Rev. **111**, 929 (1958).
22. F. Froehner, *JEFF Report* 18 (2001), see eq. (196).
23. G. Arbanas, V. Sobes, A. Holcomb, P. Ducru, M. Pigni, D. Wiarda, EPJ Web of Conferences **146**, 12006 (2017).
24. S. Kunieda, EPJ Web of Conferences **146**, 12029 (2017).
25. E.P. Wigner, L. Eisenbud, Phys. Rev. **72**, 29 (1947).
26. T. Kawano, H. Matsunobu, T. Murata, A. Zukeran, Y. Nakajima, M. Kawai, O. Iwamoto, K. Shibata, T. Nakagawa, T. Ohsawa *et al.*, J. Nucl. Sci. Technol. **37**, 327 (2000).
27. R.E. Azuma, E. Uberseder, E.C. Simpson, C.R. Brune, H. Costantini, R.J. de Boer, J. Görres, M. Heil, P.J. LeBlanc, C. Ugalde *et al.*, Phys. Rev. C **81**, 045805 (2010).
28. E. Uberseder, R.J. deBoer, *AZURE2 User Manual* (2015) `azure.nd.edu`.
29. R.J. deBoer, J. Görres, M. Wiescher, R.E. Azuma, A. Best, C.R. Brune, C.E. Fields, S. Jones, M. Pignatari, D. Sayre *et al.*, Rev. Mod. Phys. **89**, 035007 (2017).
30. The GSL Team, *GSL 2.5 Documentation* (2018) `https://www.gnu.org/software/gsl/doc/`.
31. N. Michel, Comput. Phys. Commun. **176**, 232 (2007).
32. Minuit2, release 2008, `http://seal.web.cern.ch/seal/snapshot/work-packages/mathlibs/minuit/`.
33. G. D'Agostini, Nucl. Instrum. Methods Phys. Res. A **346**, 306 (1994).
34. L. Wolfenstein, Annu. Rev. Nucl. Sci. **6**, 43 (1956).
35. R. Newton, *Scattering Theory of Waves and Particles, Dover Books on Physics* (Dover Publications, 2002).
36. I.J. Thompson, Comput. Phys. Rep. **7**, 167 (1988).
37. Fresco coupled reaction channels calculations (2006) `www.fresco.org.uk`.
38. Scattering code FRESCO for coupled-channels calculations (2017) `https://github.com/I-Thompson/fresco`.
39. A. Koning, S. Hilaire, S. Goriely, *TALYS - A nuclear reaction program* (2015) `http://www.talys.eu/home/`.
40. I. Thompson, A. Barnett, Comput. Phys. Commun. **36**, 363 (1985).
41. B. Adams, L. Bauman, W. Bohnhoff, K. Dalbey, M. Ebeida, J. Eddy, M. Eldred, P. Hough, K. Hu, J. Jakeman *et al.*, *DAKOTA, A Multilevel Parallel Object-Oriented Framework for Design Optimization, Parameter Estimation, Uncertainty Quantification, and Sensitivity Analysis: Version 5.4 User's Manual*, Sandia Technical Report SAND2010-2183 (2009), updated April 2013.

42. N.M. Larson, Technical Report ORNL/TM-9179/R8, Oak Ridge National Laboratory (2008).
43. P. Archier, C. De Saint Jean, O. Litaize, G. Noguère, L. Berge, E. Privas, P. Tamagno, Nucl. Data Sheets **118**, 488 (2014).
44. J. Raynal, Technical Report CEA-N-2772, pp. 1–145, Commissariat à l'Énergie Atomique, Saclay, France (1994).
45. B. Habert, C. De Saint Jean, G. Noguère, L. Leal, Y. Rugama, Nucl. Sci. Eng. **166**, 276 (2010).
46. M. Herman, A. Trkov, *ENDF-6 Formats Manual*, (Brookhaven National Laboratory, 2009) bNL-90365-2009.
47. B. Beck, C. Mattoon, Technical Report, Lawrence Livermore National Laboratory (2014) lLNL-PROC-648476.
48. C. Mattoon, B. Beck, N. Patel, N. Summers, G. Hedstrom, D. Brown, Nucl. Data Sheets **113**, 3145 (2012).
49. F. Barker, Aust. J. Phys. **25**, 341 (1972).
50. N. Otuka, E. Dupont, V. Semkova, B. Pritychenko, A. Blokhin, M. Aikawa, S. Babykina, M. Bossant, G. Chen, S. Dunaeva *et al.*, Nucl. Data Sheets **120**, 272 (2014).
51. R.J. Spiger, T.A. Tombrello, Phys. Rev. **163**, 964 (1967).
52. A. Barnard, C. Jones, G. Phillips, Nucl. Phys. **50**, 629 (1964).
53. T.A. Tombrello, P.D. Parker, Phys. Rev. **130**, 1112 (1963).
54. J.A. McCray, Phys. Rev. **130**, 2034 (1963).
55. A.J. Elwyn, R.E. Holland, C.N. Davids, L. Meyer-Schützmeister, F.P. Mooring, W. Ray, Phys. Rev. C **20**, 1984 (1979).

IAEA Collaboration on R-matrix codes.